Three-dimensional fabrication and characterisation of core-shell nano-columns using electron beam patterning of Ge-doped SiO_2

Lionel C. Gontard[1], Joerg R. Jinschek[2], Haiyan Ou[3], Jo Verbeeck[4] and Rafal E. Dunin-Borkowski[5]

1 Instituto de Ciencia de Materiales de Sevilla (CSIC), 41092, Sevilla, Spain
2 FEI Europe, Achtseweg Noord 5, 5600 KA Eindhoven, The Netherlands
3 Department of Photonics, Technical University of Denmark, DK-2800 Kongens Lyngby, Denmark
4 EMAT, University of Antwerp, Groenenborgerlaan 171, B-2020 Antwerp, Belgium
5 Ernst Ruska-Centre for Microscopy and Spectroscopy with Electrons and Peter Grünberg Institute, Forschungszentrum Jülich, D-52425 Jülich, Germany

A focused electron beam in a scanning transmission electron microscope (STEM) is used to create arrays of core-shell structures in a specimen of amorphous SiO_2 doped with Ge. The same electron microscope is then used to measure the changes that occurred in the specimen in three dimensions using electron tomography. The results show that transformations in insulators that have been subjected to intense irradiation using charged particles can be studied directly in three dimensions. The fabricated structures include core-shell nano-columns, sputtered regions, voids and clusters.

The scanning transmission electron microscope is a versatile instrument, which can be used to illuminate a thin specimen with a focused beam of electrons to detect the scattered electron intensity to form an image. Besides providing useful information about the specimen, the electron beam used in an electron microscope can be used to cause either temporary or permanent changes to its surface or bulk structure. The incident electron beam can result in defect formation, mass loss, atom displacement, phase transitions, a change in temperature and the presence of an electric field, arising

both from the electron beam itself and from charging of the specimen.[1,2,3] In this work, we directly examine in three spatial dimensions the local transformations that are induced in a sample that is irradiated selectively.

We used a probe-aberration-corrected FEI Titan field-emission gun transmission electron microscope (FEG TEM) operated in scanning mode to both pattern and image a thin insulating Ge-doped SiO_2 specimen. Electron irradiation of the specimen results in the build-up of an electric field, ionization and displacement of dopant atoms, i.e., electromigration[4]. The electron dose determines the rate of decrease of the local charge density when the source of electrons is turned off, allowing electromigration to be suppressed by using intermittent electron irradiation. Images of a specimen can then be acquired non-invasively using short dwell times (or fast scanning of the beam). Figures 1(a) and 1(c) show high-angle annular dark-field (HAADF) STEM images of a 200-nm-thick Ge-doped SiO_2 specimen that has been irradiated using a 200 keV electron beam (Figure 1(d)). The arrays of dark circles with white borders correspond to the locations at which the beam was stopped. As will be shown below, these circles are in fact cylinders that pass through the full specimen thickness and are viewed in projection. The different diameters of the circles in Figure 1(c) result from the use of different irradiation times, between 1 ms and 24 s, or equivalently to different electron doses. The diameters reach a steady value of 10-12 nm after 8-24 s of irradiation. The bright shells surrounding the circles, which are indicative of a material that has a higher atomic number or density than the surrounding SiO_2, have thicknesses in the range of 2-5 nm, which do not depend significantly on irradiation time.

The formation of the core-shell structures shown in Figure 1 is likely to be thermally and/or electrically driven.[5,6] Although SiO_2 has poor thermal conductivity, its temperature is not expected to increase significantly because of the likelihood of efficient dissipation of heat from the small illuminated area to the rest of the sample. Although electron probes with very small diameters may have high current densities, the temperature rise is typically expected to be below 20 K.[5] However, the local temperature gradient can be high, resulting in thermally-driven diffusion of atoms.[6] In order to assess the effect of temperature on the formation of the core-shell structures, localized irradiation was performed with the specimen examined at temperatures of between -178 and +150 °C. Similar structures always formed, suggesting that

temperature does not play a primary role. With respect to the electric field, when a TEM specimen is irradiated with electrons, inelastic scattering processes result in core level ionization events that are followed by Auger and secondary electron emission from the atoms in the specimen. The Auger electrons, in particular, have high kinetic energy (> 50 eV) and can escape from the attraction of the excited atoms, which may then remain in an ionic state. In an insulating material, the electrical equilibrium cannot be restored quickly and a net charge builds up in the specimen, as shown in Figure 1(f) in the form of an off-axis holography measurement of the electrostatic fringing field in the vacuum region adjacent to the present specimen during electron irradiation in the TEM [7]. The cosine of the phase was calculated to visualize equiphase lines, which provide a quantitative representation of the projected electrostatic potential. As a result of the excess positive charge in the specimen, charged species may be expelled from their initial sites. Amorphous SiO_2 may then become O-deficient, and Ge ions may be driven away from the irradiated region. At an atomic level, electron irradiation of glasses tends to eliminate non-bridging oxygen (NBO), to which cations are bound, based on the Knotek-Feibelman model for ionization, whereby the incident electron creates an inner-shell vacancy on the metal site, followed by (interatomic) Auger decay from the oxygen.[11] This results in a (neutral or) positive O atom or ion, which is repelled by the surrounding metal ions. Cations that are released from the glass network in an electron-illuminated area that is small can migrate to adjacent regions driven by a repulsive electrostatic field, leaving vacancies that are partly filled by Si and O, and O_2 can form.

Although the grey levels in Figures 1(a) and (c) are approximately proportional to the local atomic number squared, the images do not provide direct compositional information. Therefore, the local chemical compositions of the different parts of the core-shell structures were quantified using electron energy-loss spectroscopy (EELS) and energy-dispersive X-ray spectroscopy (EDXS). In order to measure the compositions of the fabricated nanostructures without altering the specimen composition, the beam was rastered rapidly during the measurements. Elemental quantification of EELS spectra was performed using *EELS Model* software.[10] Zero-loss peaks were acquired in vacuum for deconvolution, the spectra were corrected for plural scattering and the known composition of the matrix was used as a check in the quantification of the compositions of the shells and the cores. EDXS spectra were quantified using *TIA* software. [26] The measurements in Figure 1(b) show that the Ge

content increases at the shells at the expense of the cores, while the Si content is reduced in the shells but remains similar to the Ge content at these locations.[11] The measurements indicate that Ge has migrated from the centres of the irradiated areas to the shells, where the compositional ratios for O:Ge and O:Si suggest a mixed oxide composition of GeO_2 and SiO_2. [13,14]

HAADF STEM tomography was used to reconstruct a three-dimensional representation of the irradiated specimen from a tilt-series of two-dimensional projections like the one shown in Figure 2(b) corresponding to a tilt of 0 degrees.[7,8,9] Tomographic series were acquired by tilting the specimen inside the microscope over a range of 140°. Alignment and reconstruction of the volume was performed using *Inspect3D* software and the simultaneous iterative reconstruction (SIRT) algorithm (10 iterations proved to be sufficient to achieve convergence).[26] Figures 2(a) and (c) show different views of the three-dimensional volume of the irradiated specimen. The visualisations reveal straight core-shell structures with cylindrical symmetry that are formed within the full depth of the specimen, as well as the presence of sputtering at the exit surface and nanoparticles close to the entrance surface (see also Figure 1(e)).

The core-shell structures are likely to have resulted from the presence of an electric field, which drives the electromigration of mobile Ge ions. Following the theoretical models of Cazaux[4] the electric field associated with a uniform charge distribution created by a stationary electron beam incident normal to the specimen surface can be described in terms of a radial and an axial component. The radial component is greatest at a distance from the centre equal to the electron-beam radius, after which it decreases exponentially with distance. This dependence accounts for the fact that the cylinders have diameters that are much larger than the ~0.3 nm size of the electron beam used. The axial component of the electric field (in the electron beam direction) changes sign at the midpoint of the specimen and increases linearly towards its surfaces. The uniformity of the shells observed in our experiments indicates that the drift of Ge ions is overwhelmingly perpendicular to the electron beam direction at all depths in the specimen, in agreement with a theoretical model predicting that the radial component of the field is much higher than the axial component in a thin unsupported uncoated insulator. The sputtered areas that are observed experimentally at the exit surface of the

specimen are likely to result from elastic scattering of atoms into the vacuum of the microscope.

The tomographic data (Figures 2(a) and (c)), high-resolution STEM, EDXS microanalysis and atomic force microscopy (AFM) data also revealed the presence of Ge nanoparticles with an average size of 2-6 nm close to the specimen surfaces (see Supplementary information). Ge clusters have previously been observed to form in Ge-doped glasses irradiated with broad electron probes or following thermal heating.[14,15] Such materials exhibit efficient luminescence and are capable of storing electrical charge, with potential applications in optoelectronics,[16,17] depending on the morphologies and the spatial distributions of the nanocrystals. Electron tomography provides valuable information about these parameters, suggesting here that surface effects (the nanoparticles form preferentially at the surface) may have a significant effect on the optical/electrical properties of such samples. The nanoparticles that are observed on the surface of the sample may have formed when the sample was prepared for TEM examination after annealing or during observation in the TEM.

For comparison with the nanofabricated patterns obtained using high-energy electrons, a scanning electron microscope (SEM) equipped with a field emission electron gun was also used to irradiate the thin sample at an accelerating voltage of 30 kV using a current density of 318 pA/Å^2. HAADF STEM tomography was again used to measure the resulting changes inside the sample (Figure 3(a)) after irradiating the specimen with the SEM at a single point (Figure 3(b)). Close to the entrance surface, a core-shell structure formed, as in the STEM experiment, although with a larger diameter, resulting from the larger diameter and higher current of the incident electron beam. Interestingly, deeper in the specimen, large spherical voids surrounded by a thin Ge-rich shell are observed. As in the STEM experiment, O diffusion is likely to be electrically driven and can form O_2. If the pressure and temperature increase locally, then gas bubbles of O_2 can grow and finally burst. Irrespective of the electron dose, we never observed the formation of bubbles during irradiation in the TEM. The current density used in the SEM was 3 times higher than that in the TEM, suggesting that the dose rate is important, probably combined with the effect of temperature. The incident electron energy is also lower in the SEM compared to that in the TEM. Therefore, if the electron scattering range is smaller than the film thickness, then all of the beam energy will be deposited in the

specimen, increasing the local temperature. In some cases, the local specimen temperature may reach a few hundred degrees for a stationary probe (e.g., in an organic specimen).[18,19] The results shown in Fig. 3 are consistent with such a mechanism.

The present results show that the effects of irradiation on materials can be measured in three dimensions with high spatial resolution using HAADF STEM tomography by adjusting the dwell time to avoid further damage to the material during subsequent imaging. The electron beam in an electron microscope can be used to create regular arrays of core-shell cylinders with well-defined diameters and pitches. In some of the core-shell structures a "coaxial"-like structure is observed (see Supplementary information). These structures can have the topology of photonic crystals on the nanometer scale and may be important for tailor-made electronic and/or optical devices such as plasmonic sensors or transistors.[20-24] They are also playgrounds for studying physics in quasi-onedimensional systems.[25] Our results are also important for technological and scientific applications in which insulating materials are irradiated with highly energetic charged particles. For example, proton beams are used in the treatment of human cells, insulating materials are used as protective layers in fusion and fission reactors and semiconductors are routinely used for detecting particles in high-energy physics.

References

1. R. F. Egerton, F. Wang and P. A. Crozier, Microsc. Microanal. **12**, 65 (2006).

2. G. S. Chen, C. B. Boothroyd and C. J. Humphreys, Philos. Mag. A **78**, 491 (1998).

3. S. B. Fischer, Radiat. Eff. **5**, 239 (1990).

4. J. Cazaux, J. Appl. Phys. **59**, 1418 (1986).

5. G. Möbus, M. Ojovan, S. Cook, J. Tsai and G. Yang J. Nucl. Mater. **396**, 264 (2010).

6. W. Shockley, Phys. Rev. **93**, 345 (1954).

7. P. A. Midgley and R. E. Dunin-Borkowski, *Nature Mater.* **8**, 271 (2009).

8. L. C. Gontard, R. E. Dunin-Borkowski and D. Ozkaya, J. Microsc. **232**, 248 (2008).

9. L. C. Gontard, R. E. Dunin-Borkowski, M. H. Gass, A. L. Bleloch and D. Ozkaya, J. Electron Microsc. **58**, 167 (2009).

10. J. Verbeeck and S. Van Aert, Ultramicroscopy, **101**, 207 (2004).

11. N. Jiang, G. G. Hembree, J. C. H. Spence, J. Qiu, F. J. Garcia de Abajo and J. Silcox, Appl. Phys. Lett. **83**, 551 (2003).

12. M. L. Knotek and P. J. Feibelman, Phys. Rev. Lett. **40**, 964 (1978).

13. M. Klimenkov, W. Matz, S. A. Nepijko and M. Lehmann, Nucl. Instrum. Meth. B **179**, 209 (2001).

14. G. S. Henderson, D. R. Neuville, B. Cochain and L. Cormier, J. Non-Cryst. Solids **355**, 468 (2009).

15. E. S. Marstein, A. E. Gunnæs, U. Serinvan, R. Turan, A. Olsen and T. G. Finstad, Surf. Coat. Tech. **158-159**, 544 (2002).

16. A. V. Kolobov, S. Q. Wei, W. S. Yan, H. Oyanagi, Y. Maeda and K. Tanaka, Phys. Rev. B **67**, 195314 (2003).

17. L. Ding, T. P. Chen, M. Yang, J. I. Wong, Y. Liu, S. F. Yu, F. R. Zhu, M. C. Tan, S. Fung, C. H. Tung and A. D. Trigg, Appl. Phys. Lett. **90**, 103102 (2007).

18. R. F. Egerton, P. Li and M. Malac, Micron **35**, 399 (2004).

19. E. S. Marstein, A. E. Gunnæs, U. Serincan, S. Jørgensen, A. Olsen, R. Turan and T. G. Finstad, Nucl. Instrum. Meth. B **207**, 424 (2003).

20. J-G. Huang, C-L. Lee, H-M. Lin, T-L. Chuang, W-S. Wang, R-H. Juang, C-H. Wang, C. K. Lee, S-M. Lin and C.-W. Lin, Biosens. Bioelectron. **22**, 519 (2006).

21. D.-Z. A. Chen, R. Hamam, M. Soljačić, J. D. Joannopoulos and G. Chen, Appl. Phys. Lett. **90**, 181921 (2007).

22. X. Peng and I. Kamiya, Nanotechnology **19**, 315303 (2008).

23. L. J. Lauhon, M. S. Gudiksen, D. Wang and C. M. Lieber, Nature **420**, 57 (2002).

24. G. Liang, J. Xiang, N. Kharche, G. Klimeck, C. M. Lieber and M. Lundstrom, Nano Lett. **7**, 642 (2007).

25. Y. Wang, N. Yang and J.-. L. Zhu, Phys. Rev. B **74**, 035432 (2006).

26. Details about *TIA* and *Inspect 3D* software can be found at the webpage of the manufacturer FEI.

KEYWORDS: transmission electron microscopy, electron irradiation, glasses, nanofabrication, voids, Ge-doped SiO_2

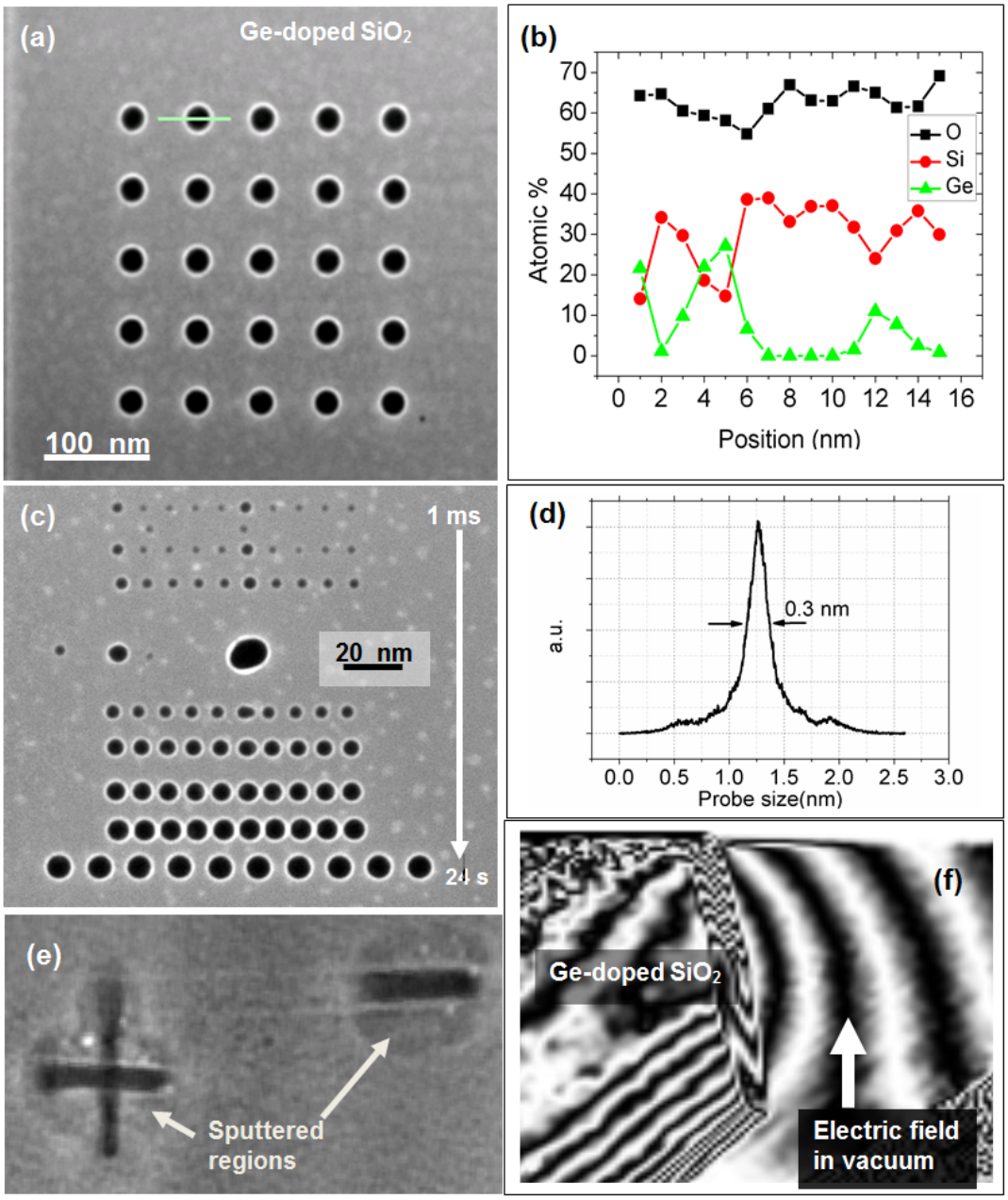

FIGURE 1. Transformation of Ge-doped SiO_2 by 200 keV electron radiation: (a) HAADF STEM image of cylinders formed after localised irradiation. (b) Elemental composition measured using EDXS along the marked line crossing one circle in (a). Si and Ge are anti-correlated at the positions of the bright rings. (c) HAADF STEM image showing the dependence of cylinder diameter on irradiation time. (d) Intensity profile of the electron beam used to pattern the cylinders in the present experiments. (e) Exit surface of the sample extracted from the tomographic reconstruction (Figure 2) showing a darker halo around the structures, suggesting that some material has been sputtered from the sample. (f) Reconstructed phase image (cosine of the phase) acquired using off-axis electron holography. The presence of black and white fringes in the vacuum region indicates that the sample has becomed electrically charged due to irradiation by the electron beam.

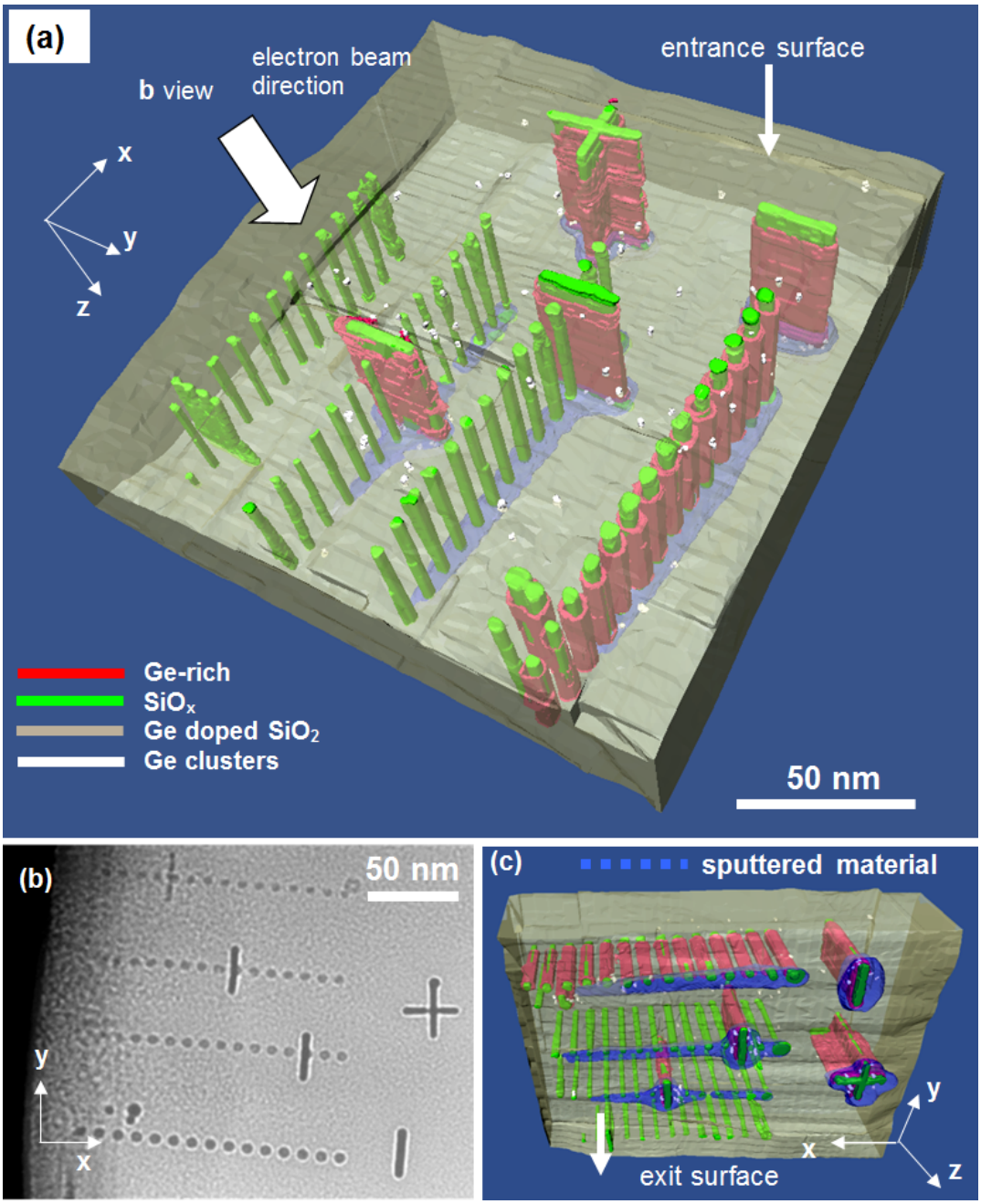

FIGURE 2. Characterisation of arrays of core-shell nanocolumns in Ge-doped SiO_2: (a) Three-dimensional visualisation of nanostructures of different diameters created by electron irradiation (accelerating voltage 200 keV; probe size 0.3 nm, current density 85 pA/Å^2 irradition time between 1 and 8 s. The reconstructed volume was segmented manually. The dimensions and distributions of core-shell structures (green and red), sputtered craters (blue), and nanoparticles (white) are visible. (b) HAADF STEM image acquired at a specimen tilt angle of 0°, taken from the tomographic tilt series. (c) View of the reconstruction from the exit surface of the specimen (see also Fig. 1(e)).

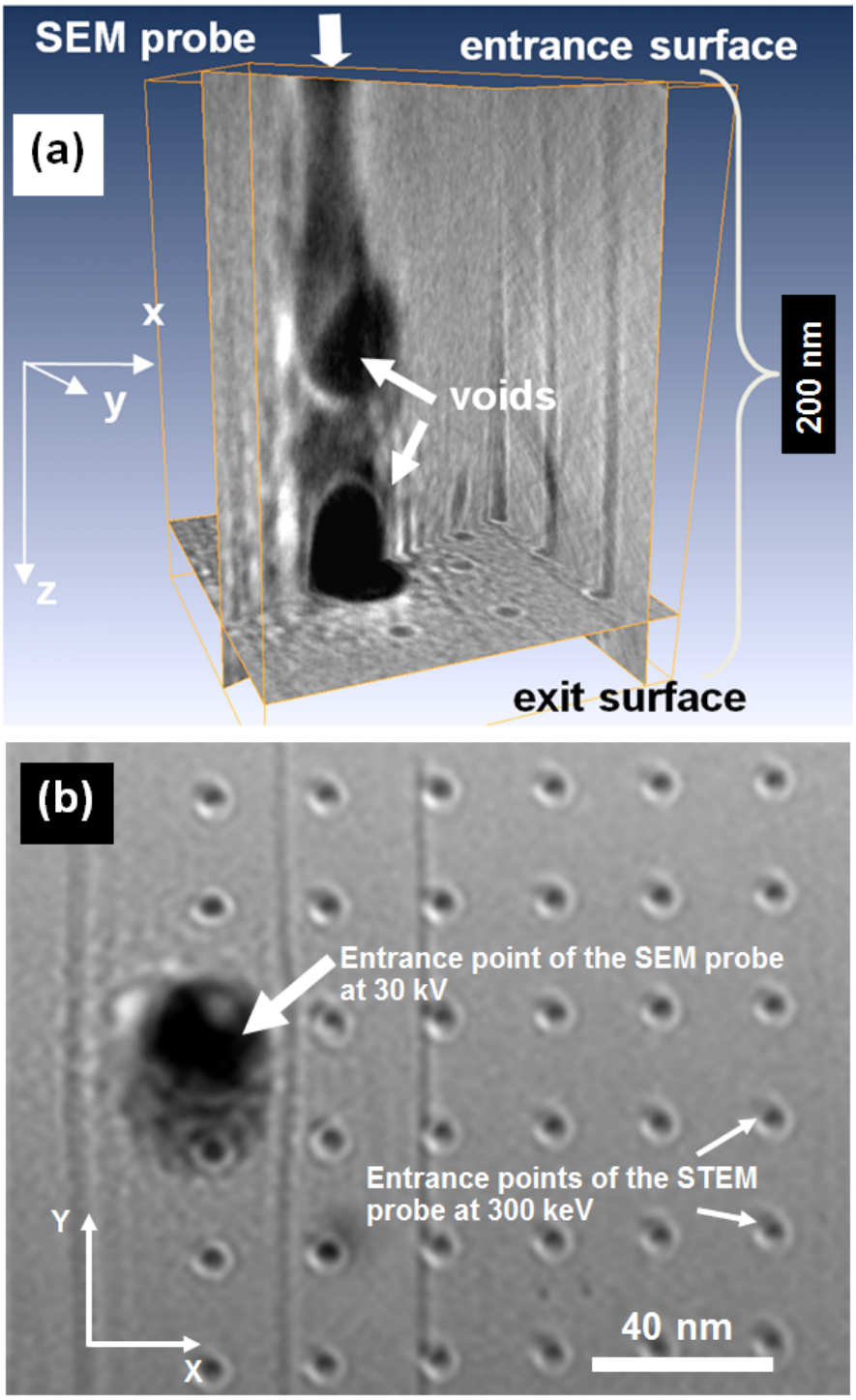

FIGURE 3. Three-dimensional visualisation of the Ge-doped SiO_2 specimen after electron irradiation in the SEM: (a) Three orthogonal sections of an HAADF STEM tomographic reconstruction of the irradiated specimen, illustrating the effects of accelerating voltage. The gray level depends on the local density and composition of material. For irradiation by electrons at 30 keV, bubbles of oxygen are thought to burst, creating voids. (b) HAADF STEM image of one point irradiated with the electron beam at 30 keV (indicated by the white arrow), surrounded by an array of points formed when the sample is irradiated with 300 keV electrons.

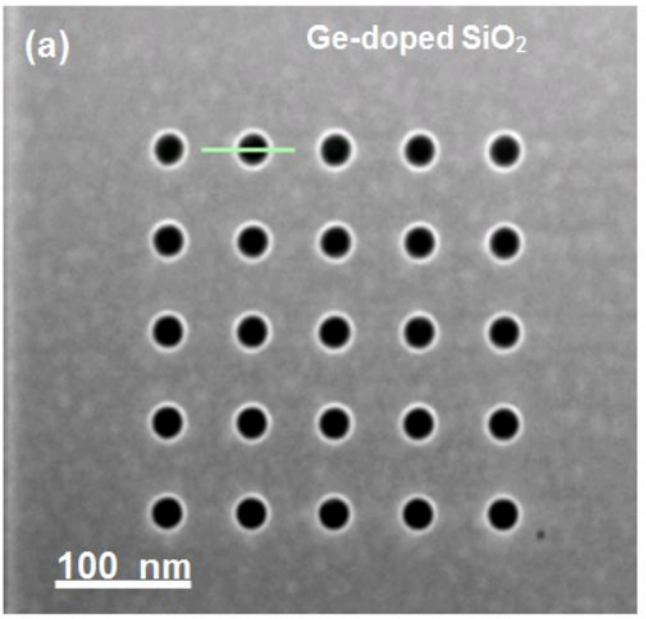
(a)
Ge-doped SiO2
100 nm

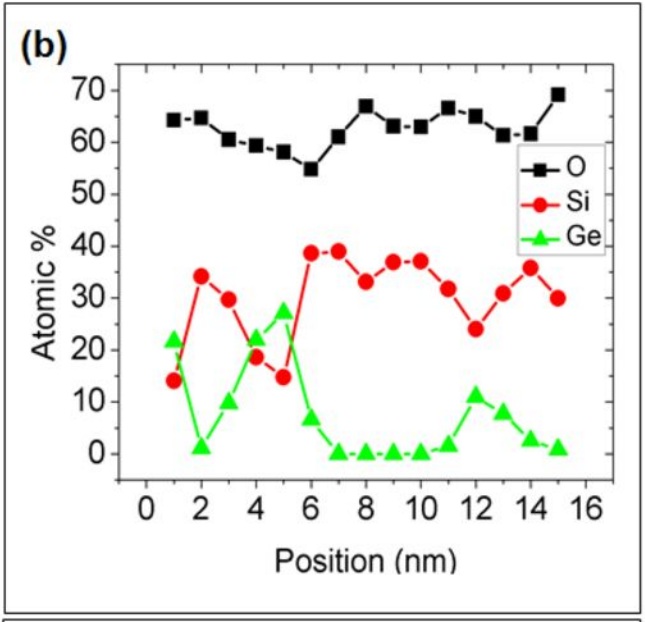
(b)
Atomic %
Position (nm)
O
Si
Ge

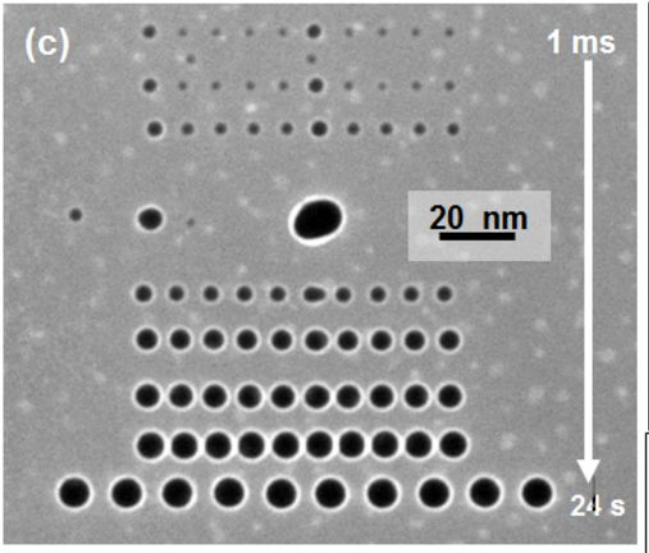
(c)
1 ms
20 nm
24 s

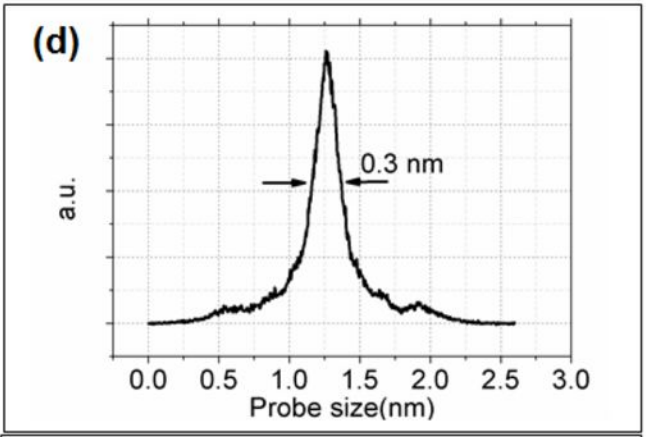
(d)
a.u.
0.3 nm
Probe size(nm)

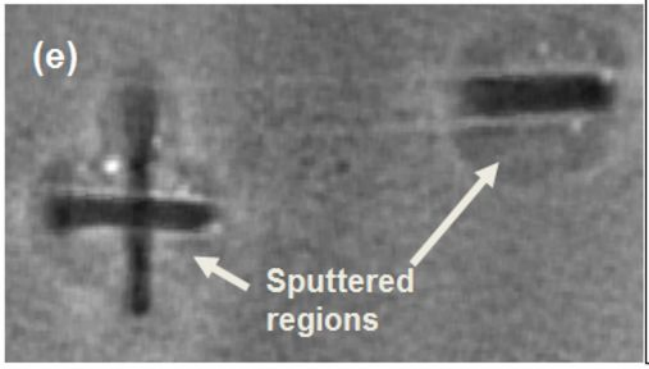
(e)
Sputtered regions

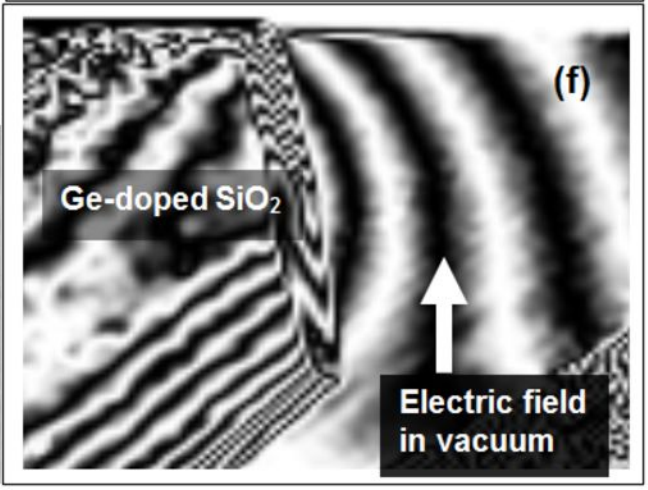
(f)
Ge-doped SiO2
Electric field in vacuum

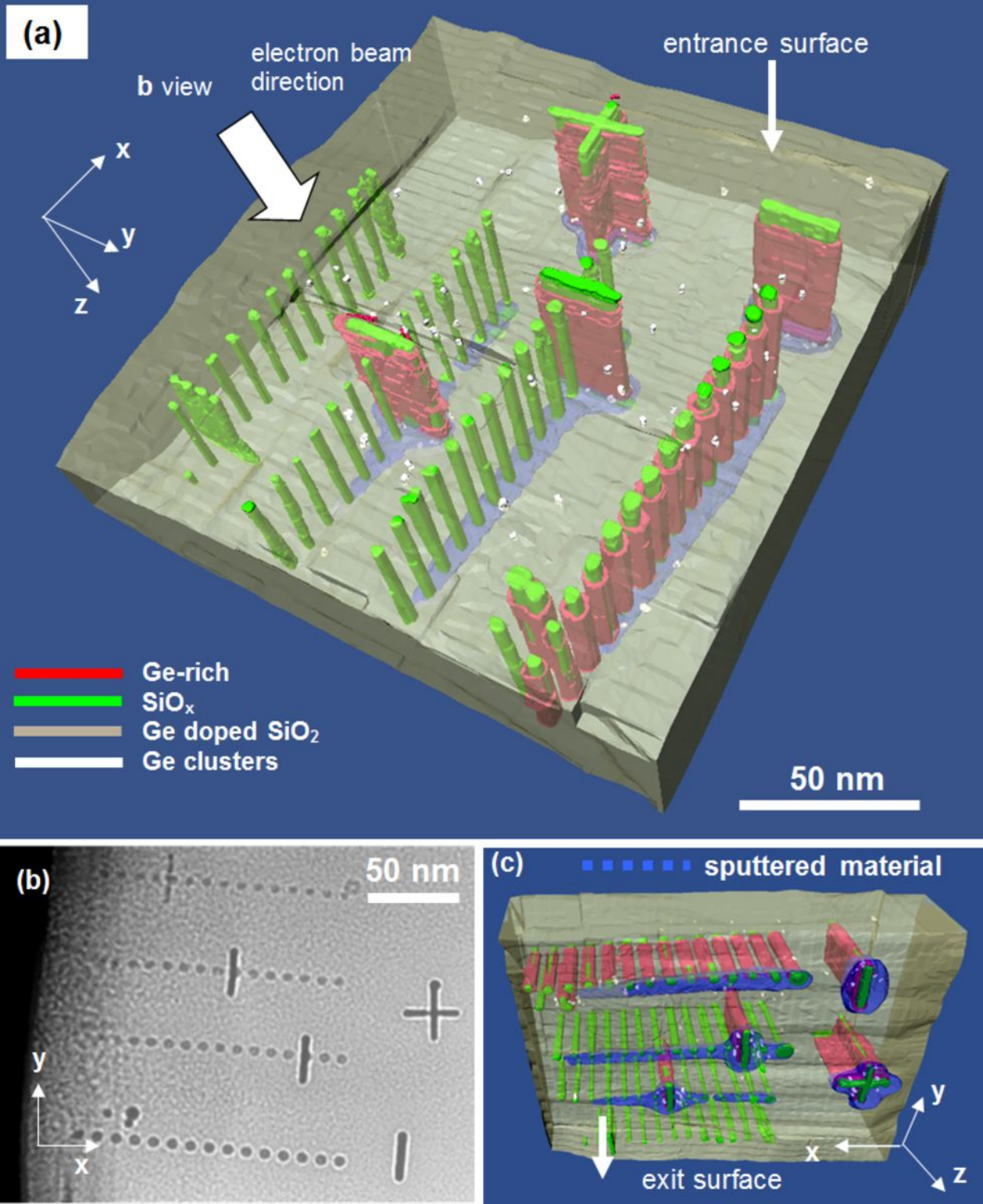
(a)
b view
electron beam direction
entrance surface
x
y
z
Ge-rich
SiOx
Ge doped SiO2
Ge clusters
50 nm
(b)
50 nm
y
x
(c)
sputtered material
exit surface
y
x
z

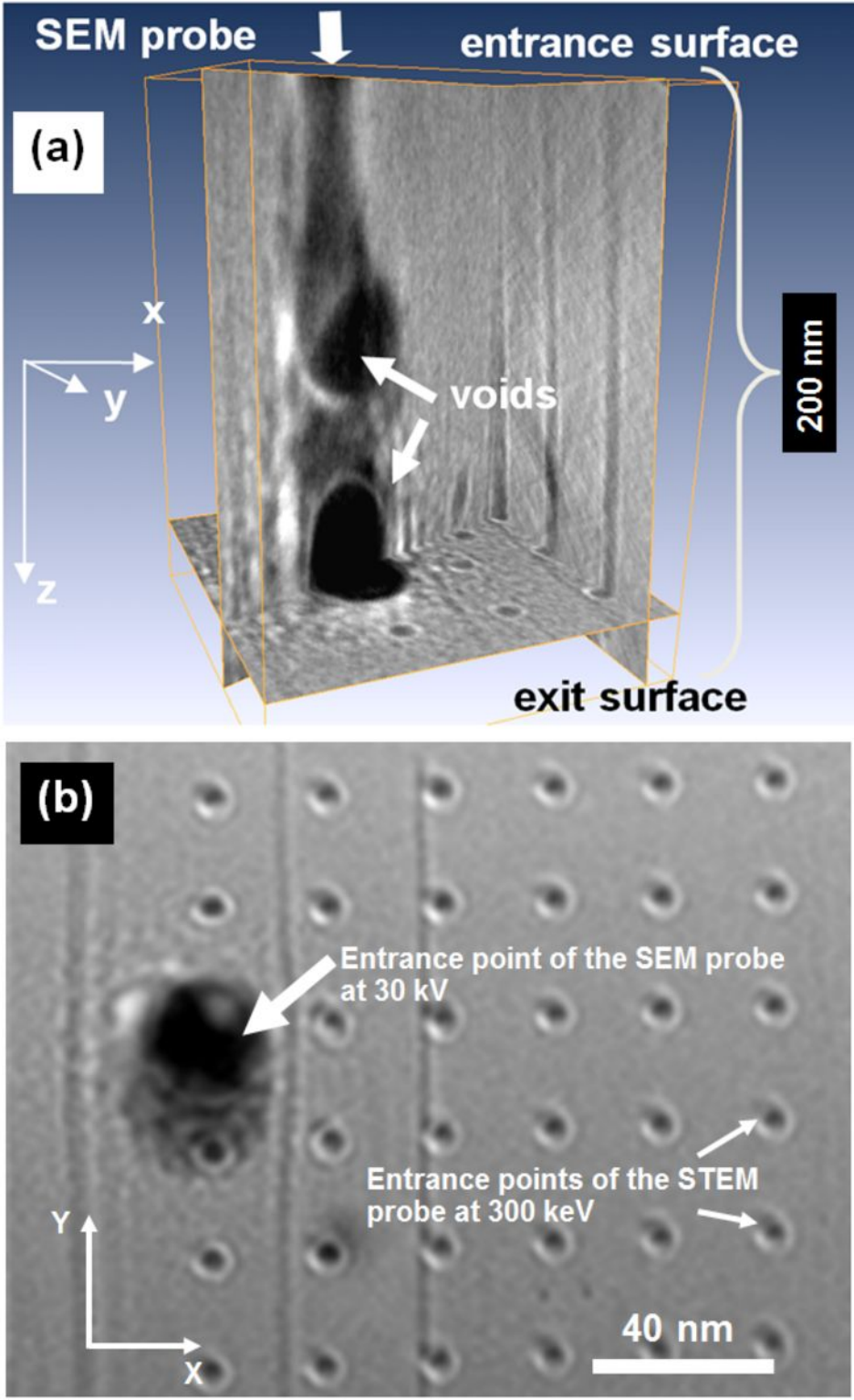
SEM probe
entrance surface
(a)
x
y
z
voids
200 nm
exit surface
(b)
Entrance point of the SEM probe at 30 kV
Entrance points of the STEM probe at 300 keV
Y
X
40 nm